# Numerical Simulation of Airflow and Airborne Pathogen Transport in Aircraft Cabins—Part I: Numerical Simulation of the Flow Field

**C.-H. Lin, PhD, PE**
*Member ASHRAE*
**R.H. Horstman, PE**
*Member ASHRAE*
**M.F. Ahlers**
**L.M. Sedgwick, PE**
**K.H. Dunn**
**J.L. Topmiller**
**J.S. Bennett, PhD**
*Associate Member ASHRAE*
**S. Wirogo, PhD**

## ABSTRACT

*An initial study to develop a numerical tool using computational fluid dynamics (CFD) methods for investigating the potential of disease transmission in commercial aircraft is completed. To gain insight of the general airflow pattern, a detailed CFD model of a small section in the passenger cabin of a B767-300 passenger cabin was built and a Reynolds-averaged Navier-Stokes (RANS) simulation was performed. By comparing with the available test data, the RANS simulation substantially underpredicted the turbulence intensity, especially in and around the breathing zone. A separate large eddy simulation (LES) was conducted to obtain a more realistic turbulent energy transport in a generic cabin model. The LES-predicted turbulence level is in fairly good agreement with the test data. Based on the LES results, the k and ε equations used in the RANS simulation were modified by using a special user subroutine. A RANS simulation with adjusted turbulence was then employed to simulate the dispersion of airborne pathogen in the detailed passenger cabin model. These adjustments allow for the simulation of disease transmission using less than 1/100 of the computing hardware resources required for an equivalent LES of airflow and particle transport.*

## INTRODUCTION

Applications of computational fluid dynamics (CFD) in studying airflow and heat transfer in ventilated rooms were incepted nearly three decades ago (Nielsen 1974). Scalar species transport was later added to address indoor air quality issues by researchers (Murakami et al. 1988; Horstman 1988; Chen et al. 1990). Haghighat et al. (1989, 1990, 1992) have expanded the domain of interest to a building of multiple compartments. CFD has since been used to evaluate the indoor environment of various types of buildings, as reported by Chen and Srebric (2001). Numerical studies dedicated to the contaminant transport in hospital operating rooms have been conducted by Lo (1997). To improve occupant thermal comfort, CFD has been used to modify and/or optimize the air ventilation system in automotives (Lin et al. 1992) and commercial airplanes (Aboosaidi et al. 1991; Baker et al. 2000).

CFD techniques used in this study varied. Baker et al. (2000) analyzed complex aircraft interiors using a laminar flow simulation. Like most reported work, Mizuno and Warfield (1992) and Aboosaidi et al. (1991) both applied the Reynolds-averaged Navier-Stokes (RANS) approach to look at velocity fields but did not address the species transport issues. To accurately predict the turbulence levels in room airflow, Emmerich and McGrattan (1998) and Zhang and Chen (2000) have used a large eddy simulation (LES) technique. Due to the relatively large physical dimensions involved in air ventilation flows, direct numerical simulation (DNS) is still prohibitively expensive to pursue with the currently available computing resources.

Airplane cabin airflow has the characteristics of very high turbulence levels with transitional Reynolds numbers. It is not always the case; however, a majority of known turbulence models used in RANS simulations underpredict the turbulence levels to various degrees (Jin and Braza 1994; Robinson and Hassan 1997). Therefore, the greatest hurdle in accurately predicting the airborne pathogen diffusion lies in realizing the very large turbulence levels that occur in aircraft cabins. Since diffusion is dominated by turbulence, an accurate prediction of turbulence is required.

**Chao-Hsin Lin, Raymond H. Horstman,** and **Leigh M. Sedgwick** are associate technical fellows and **Mark F. Ahlers** is a lead engineer at Boeing Commercial Airplanes Group, Seattle, Wash. **Kevin H. Dunn** is an environmental engineer, **Jennifer L. Topmiller** is a mechanical engineer, and **James S. Bennett** is a service fellow at the National Institute for Occupational Safety and Health, Cincinnati, Ohio. **Sutikno Wirogo** is a support engineer at Fluent, Inc., Lebanon, NH.

The objective of this part of our study is to provide a realistic simulation of the flow field in an aircraft cabin using CFD. The B767-300 was chosen as the representative airplane cabin. The method used focused on the implementation of a commercially available code, with adjustments made to the predicted diffusion to more accurately match test and LES data. LES was used as a predictive tool for turbulence levels by comparison to a relatively scarce set of test data of cabin airflow. However, LES modeling of a passenger cabin is not practical due to intensive computing requirements. For example, an LES model for one seat row of a passenger cabin of a B767-300 airplane would require 1000 gigabytes of RAM. In fact, even grids built for RANS models are barely within the available resource limits for just two seat rows of a B767-300 passenger cabin. For the turbulence study, we were unable to build an LES model of a real airplane cabin because of the aforementioned resource constraints. Instead, a simplified geometry was conceived that retains the transitional nature of the flow but with orthogonal geometry that is more amenable to the development of a highly detailed grid. The rationale is that if the turbulence levels from the simplified geometry LES model match those measured in the airplane cabin, then model adjustments could be made on a more complete set of data available from the LES results.

## GENERAL AIRFLOW PATTERN IN A B767-300 PASSENGER CABIN

To obtain the general airflow pattern in a B767-300 passenger cabin, a three-dimensional CFD model of a B767-300 cabin section (38.7 in. long) was built for this transient RANS simulation, as shown in Figure 1.

In order to preserve the geometric fidelity of the model and to keep the modeling time reasonable, hexahedral elements (424,704 cells) are used in the nozzle section and tetrahedral elements (2,229,013 cells) in the cabin section.

The ground conditions ($P_{static}$ = 14.7 psia, $T_{inlet}$ = 51°F) are specified for the simulation. The total air inflow is 94.9 cfm. Velocity inlet boundary conditions are imposed at the four nozzle inlets and static boundary conditions at the six return air grills. An assumption was made that axial flow is negligible and a symmetrical boundary condition was set at the FWD and AFT faces of the model.

Seven numerical probes are placed at the locations indicated, as detailed by Lin et al. (2001), to monitor air movement across the center plane in the cabin section.

To study the unsteadiness of airflow movement in the cabin, a steady-state flow field was needed as the initial condition for the subsequent transient simulation. The RANS equations are solved using a commercial flow solver. Simultaneously, the turbulence-caused closure problem is addressed by solving the equations of the renormalization group k-ε (RNG k-ε) model. Note that second-order schemes in space are necessary to obtain better accuracy for the steady-state solution in this study.

Figure 2 illustrates the flow field of the steady-state solution and shows that there are two large counter-rotating recirculation zones in the cabin, located around the passenger head height level at each aisle way. As shown in Figure 2, the regions where the air velocity exceeds 100 ft/min are outside the scale for the plot and, therefore, are white in color. Note that the overall flow pattern is not symmetrical with respect to the cabin cross section even though the geometry and the boundary conditions are symmetrical. This asymmetrical flow pattern is the result of inherent unsteadiness that characterizes this type of flow regime and geometry. As shown in Figure 3, the airflow at the nozzle section also supports the observation mentioned above. Before pass-

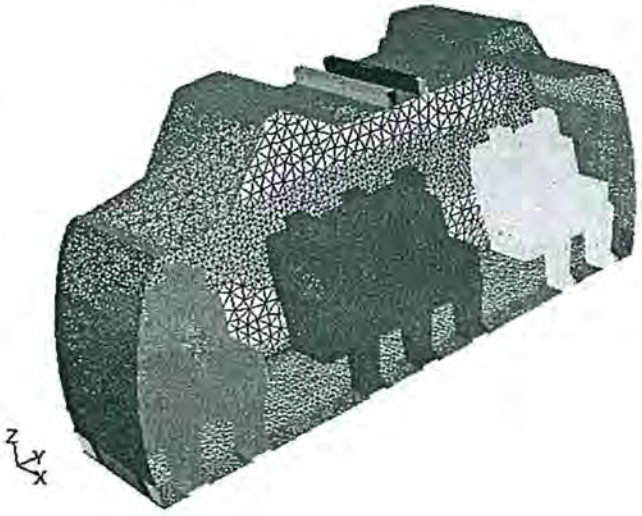


***Figure 1*** *The B767-300 cabin and nozzle model.*

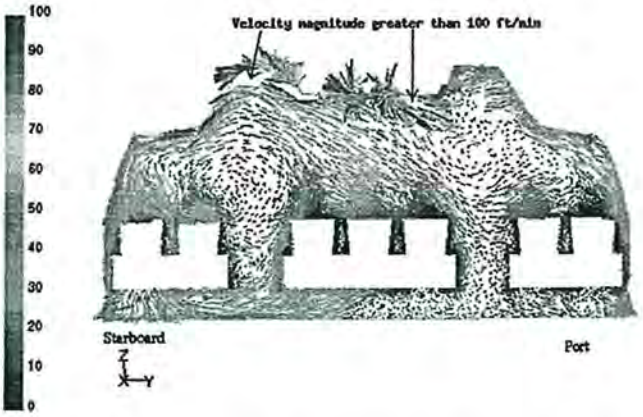


***Figure 2*** *Steady-state flow field (velocity magnitude in ft/min).*

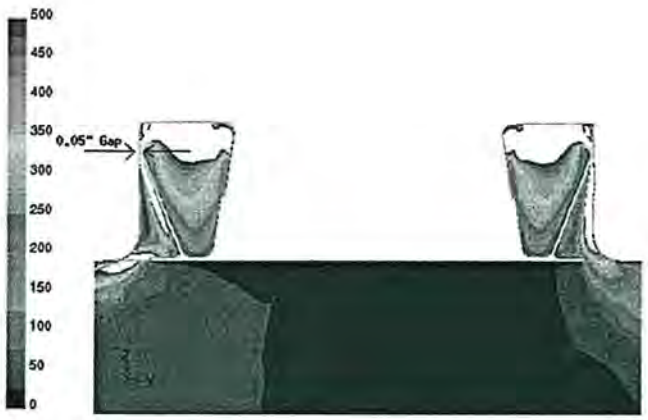


*Figure 3* *Nozzle section airflow (velocity magnitude in ft/min).*

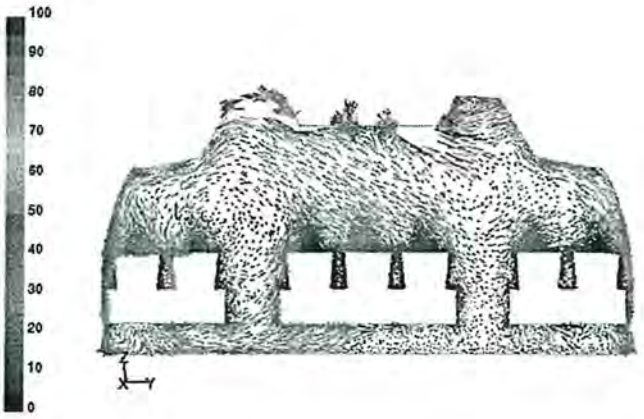


*Figure 4* *Transient flow field at* t = *14.33 seconds (velocity magnitude in ft/min).*

ing through the 0.05-in. gap, the airflow in the nozzle section is symmetrical, as shown in Figure 3. However, the airflow is separated from different walls after the gap in each of the nozzle sections. Assuming the turbulence is isotropic in this study, the fluctuating velocity component can be calculated as $v' = \sqrt{\frac{2k}{3}}$, where k is the turbulent kinetic energy. The turbulence intensity is obtained by dividing the velocity fluctuation by its mean velocity magnitude. In addition, the turbulence length scale, $l = (v')^3/\varepsilon$, where ε is the turbulence dissipation rate, is calculated. Substantial turbulence intensity (50% to 150%) is observed around the region of the two large recirculation zones, which is consistent with the measurements reported by Jones (2000). The length scale of the large eddies is about 0.5 ~ 1.0 ft.

The transient simulation is performed with a constant time step, $\Delta t = 0.001$ seconds. As previously mentioned, the lateral air movement across the symmetric plane occurs when the y-component of the air velocity at the numerical probes changes its sign (i.e., from negative to positive or vice versa). Due to the small time step and the size of the grid, we were only able to complete a time period of about 15 seconds. The swing motion across the symmetric plane is observed at one of the numerical probes at $t = 13.88$ seconds, which is consistent with the estimation of the turbulence time scale previously mentioned. At $t = 14.33$ seconds, as shown in Figure 4, the airflow pattern is developing into a more symmetrical pattern in the cabin, especially at the interfaces where the nozzle sections meet the cabin.

## THE LES RESULTS OF THE SIMPLIFIED CABIN MODEL

With RANS, the movement of large eddies in the domain of concern (which is essential for the transport of airborne pathogens) would not be resolved, as reported by Bjorn and Nielsen (1998). To capture the unsteadiness of the airflow in aircraft cabins, other CFD techniques such as DNS or LES are required.

As mentioned earlier, LES is not practical, given the available computing resources, for generating flow predictions of a model as large and complex as a B767-300 passenger cabin. For the B767-300 model, with an inlet Reynolds number ($Re_i$) of 31417, an inhibitory mesh size on the order of $(Re_i)^{9/4}$, i.e., $\sim 1.3 \times 10^{10}$ cells, is needed to do a DNS (Mathieu and Scott, 2000). The mesh requirements for an LES are approximately one order of magnitude less (about $10^9$ cells) than for the DNS (Fluent 1998). Because the smaller mesh size requirement for the LES is still far beyond the capability of available computing resources, a simplified cabin model was built to study the airflow in the cabin using this method.

As shown in Figure 5, the simplified cabin has a single slot inlet representing the interface between a nozzle and a cabin. The incoming air is set at a velocity magnitude of 2 ft/s with a slot width of 2.1 in. for a 2x slot Reynolds number of about 2500. This is typical for most airplanes supply nozzles. By preserving this transitional Reynolds number, the expectation was that the flow instability present in real cabins would also be present in the simplified model. Another important feature is the cabin scale. The seven foot dimension is representative of half of an airplane cabin cross section.

The overhead storage bins, which are normally non-rectangular in an airplane cabin, are modeled as rectangles for two reasons. First, they provide a consistent location for inlet jet separation and, second, a rectangular geometry is compatible with the most accurate meshing scheme. Non-rectangular bins can add uncontrolled instability as the jet separation point moves about. Non-orthogonal surfaces also require unnecessary numerical approximations and wall function changes that may affect stability. Note that an orthogonal geometry is also compatible with more flow solvers, especially the ones using Cartesian meshes.

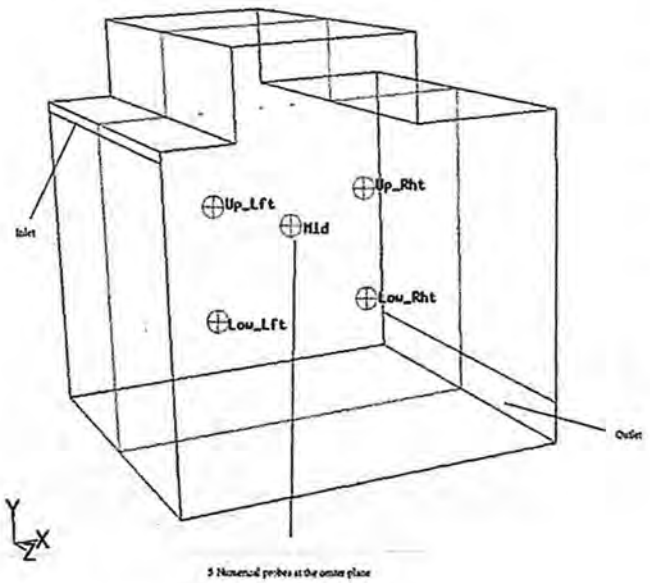


***Figure 5*** *The simplified cabin model with five numerical probes on the center plane.*

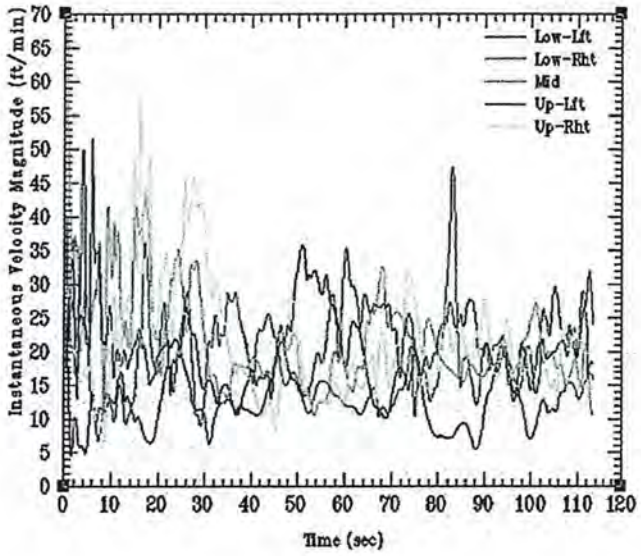


***Figure 6*** *Temporal variation of monitored |V| using a commercial code: three-dimensional LES, t = 0 to 113 seconds (velocity magnitude in ft/min).*

Two three-dimensional simplified cabin models were built to capture the large eddy motion, which is essential to predicting disease transmission via airborne routes. The velocity fluctuations observed from the original three-dimensional simplified cabin model (735,000 hexahedral cells) range between 20% and 30% of the mean air velocity after adding the contribution from the minor sub-grid motion. It was decided that the original model needed to be refined. Based on the Reynolds number at the inlet, Re = 2225, the Kolmogorov length scale, $\eta$, is 0.003 ft. Simulating the airflow in this case using a DNS requires $Re^{9/4} = 34$ million cells. To do LES for this case, the refined mesh has the grid spacing of $5 \sim 20\eta$ in all directions and consists of 2.55 million hexahedral cells.

A time step, $\Delta t = 0.05$ seconds, was selected based on the Kolmogorov time scale of the inlet $\tau = 0.059$ seconds. As shown in Figure 5, the simplified model has all of the key dimensions of a 7-ft long aircraft cabin (corresponding to the length of two seat rows with half of the cross section). Five numerical probes, denoted as "lower-left," "upper-left," "middle," "upper-right," and "lower-right" in clockwise order, are placed on the center plane to monitor the flow motion, as shown in Figure 5. At those points, the instantaneous velocity magnitude of the large eddy motion, $|\vec{V}| = |\bar{V}| + |v'|_{LES}$, is recorded at every time step. Note that the third component of the instantaneous velocity magnitude due to the sub-grid scale motion (SGS), $|v'|_{SGS}$, is not included due to its negligible contribution found in this study.

The time history of the instantaneous velocity magnitude at these locations was recorded and is shown in Figure 6. These signals were verified by a parallel LES simulation using the

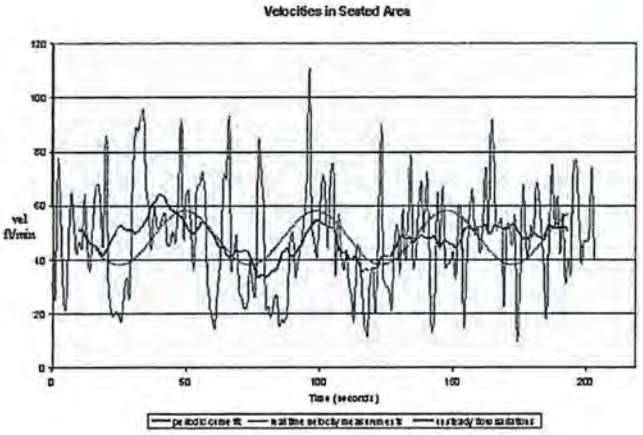


***Figure 7*** *Typical measured air velocity magnitudes in an airplane cabin seated area using hot-wire anemometer (velocity magnitude in ft/min).*

NIST-developed fire dynamics simulator (FDS), as detailed by Lin et al. (2001). Furthermore, at the five-point temporal, the predicted velocity fluctuations, from both the three-dimensional LES and the FDS LES, have shown the same turbulence level compared with the one-point hot-wire data, as shown in Figure 7. The three-dimensional LES results at $t = 113$ seconds are shown in Figure 8, and more temporal instances of the predicted flow field are available in Lin et al. (2001).

Figure 9 provides the temporal and spatial distribution of the velocity fluctuations in order to compare the instantaneous

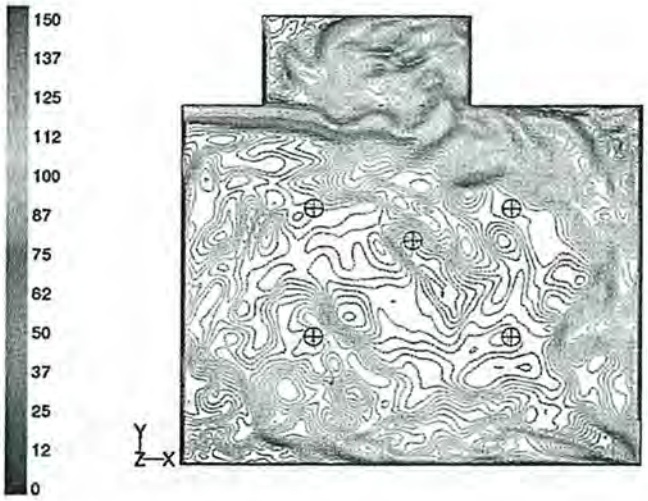


*Figure 8* *Three-dimensional flow field on center plane using LES at t = 113.47 seconds (velocity magnitude in ft/min).*

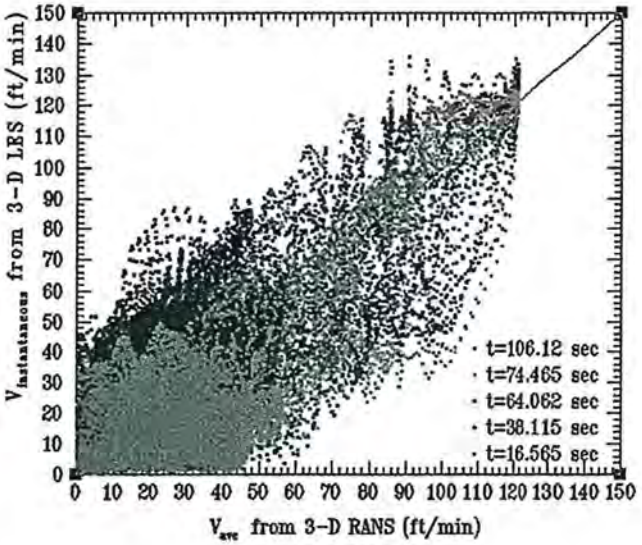


*Figure 9* $V_{instantaneous}$ *(three-dimensional LES) vs.* $V_{ave}$ *(three-dimensional RANS) over entire center plane.*

velocity magnitude (at 15,599 nodes over the entire three-dimensional LES center plane) with its steady-state three-dimensional RANS counterpart at various temporal instances. The velocity fluctuation, $v'$, predicted by three-dimensional LES ranges from 30% to 200% of its corresponding $V_{ave}$ predicted by the three-dimensional steady-state RANS simulation over the entire center plane, as illustrated in Figure 9. Using an isotropic assumption, the corresponding velocity fluctuations were calculated from the three-dimensional RANS steady-state simulation. As shown in Figure 10, $V_{ave}\pm v'$ is plotted against $V_{ave}$ over the entire center plane. Note that the steady-state RANS simulation underpredicted the velocity fluctuation, especially for the lower speeds (say, < 50 ft/min), as shown in Figure 10. The conclusion is that the RANS simulated velocity fluctuations are due to turbulent motion and should be adjusted by those obtained using the LES-predicted values.

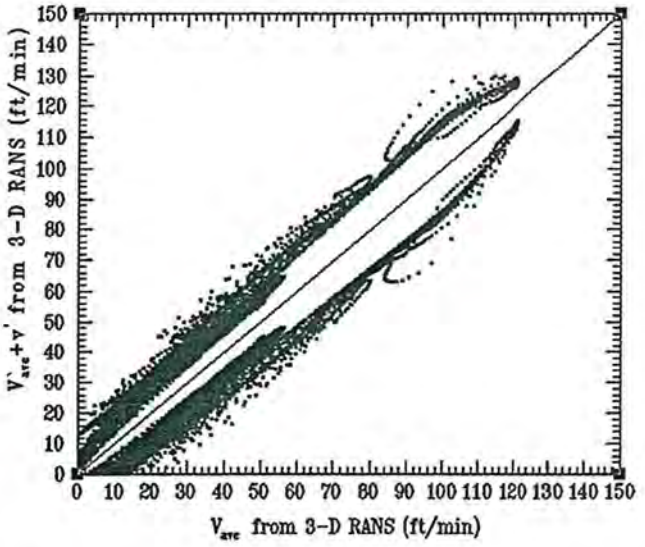


*Figure 10* $V_{ave}\pm v'$ *(three-dimensional RANS) vs.* $V_{ave}$ *(three-dimensional RANS) over entire center plane.*

## DIFFUSION ADJUSTMENTS

An example of a turbulence model is the two equation k-ε model:

The standard model:

$$\rho u\frac{\partial k}{\partial x}+\rho v\frac{\partial k}{\partial y}=\frac{\partial}{\partial x}\left[\left(\mu+\frac{\mu_t}{\sigma_k}\right)\frac{\partial k}{\partial x}\right]+\frac{\partial}{\partial y}\left[\left(\mu+\frac{\mu_t}{\sigma_k}\right)\frac{\partial k}{\partial y}\right]+\mu_t\left[2\left(\frac{\partial u}{\partial x}\right)^2+2\left(\frac{\partial v}{\partial y}\right)^2+\left(\frac{\partial u}{\partial y}+\frac{\partial v}{\partial x}\right)^2\right]-\rho\varepsilon \quad (1)$$

$$\rho u\frac{\partial \varepsilon}{\partial x}+\rho v\frac{\partial \varepsilon}{\partial y}=\frac{\partial}{\partial x}\left[\left(\mu+\frac{\mu_t}{\sigma_\varepsilon}\right)\frac{\partial \varepsilon}{\partial x}\right]+\frac{\partial}{\partial y}\left[\left(\mu+\frac{\mu_t}{\sigma_\varepsilon}\right)\frac{\partial \varepsilon}{\partial y}\right]+C_{\varepsilon 1}\mu_t\frac{\varepsilon}{k}\left[2\left(\frac{\partial u}{\partial x}\right)^2+2\left(\frac{\partial v}{\partial y}\right)^2+\left(\frac{\partial u}{\partial y}+\frac{\partial v}{\partial x}\right)^2\right]-C_{\varepsilon 2}\rho\frac{\varepsilon^2}{k} \quad (2)$$

For low Reynolds numbers:

$$\rho u\frac{\partial k}{\partial x}+\rho v\frac{\partial k}{\partial y}=\frac{\partial}{\partial x}\left[\left(\mu+\frac{\mu_t}{\sigma_k}\right)\frac{\partial k}{\partial x}\right]+\frac{\partial}{\partial y}\left[\left(\mu+\frac{\mu_t}{\sigma_k}\right)\frac{\partial k}{\partial y}\right]$$
$$+\mu_t\left[2\left(\frac{\partial u}{\partial x}\right)^2+2\left(\frac{\partial v}{\partial y}\right)^2+\left(\frac{\partial u}{\partial y}+\frac{\partial v}{\partial x}\right)^2\right]-\rho\varepsilon-2\mu\left[\left(\frac{\partial\sqrt{k}}{\partial x}\right)^2+\left(\frac{\partial\sqrt{k}}{\partial x}\right)\right] \quad (3)$$

$$\rho u\frac{\partial \varepsilon}{\partial x}+\rho v\frac{\partial \varepsilon}{\partial y}=\frac{\partial}{\partial x}\left[\left(\mu+\frac{\mu_t}{\sigma_\varepsilon}\right)\frac{\partial \varepsilon}{\partial x}\right]+\frac{\partial}{\partial y}\left[\left(\mu+\frac{\mu_t}{\sigma_\varepsilon}\right)\frac{\partial \varepsilon}{\partial y}\right]$$
$$+C_{\varepsilon 1}\mu_t\frac{\varepsilon}{k}\left[2\left(\frac{\partial u}{\partial x}\right)^2+2\left(\frac{\partial v}{\partial y}\right)^2+\left(\frac{\partial u}{\partial y}+\frac{\partial v}{\partial x}\right)^2\right]-C_{\varepsilon 2}f_2\rho\frac{\varepsilon^2}{k}+E_1 \quad (4)$$

where

$$E_1\cong 2\frac{\mu_t}{\rho}\left[\left(\frac{\partial^2 u}{\partial x^2}\right)^2+\left(\frac{\partial^2 v}{\partial x^2}\right)^2\right]$$

In each case, the pair of equations is used to produce an eddy viscosity field for the solution of the Navier-Stokes equations. Although the time-averaged velocity fields are reasonably accurate, the turbulence levels are underpredicted by approximately 1/2.82 or about 35.5%, as reported in Lin et al. (2001). In other words, the predicted levels are about 35.5% of the actual turbulence levels, as measured by $v'$.

The turbulence models in commercial software packages allow for some adjustment of the constants shown in the two equations. Unfortunately, none of the constants available could be adjusted to produce ample turbulent kinetic energy above the levels predicted by the standard model. A proprietary code, KEYO, does allow for the adjustment of all constants within the two equations, plus the addition of others is possible. The philosophy behind the adjustment is to increase the kinetic energy of turbulence $k$, in the first equation and increase the dissipation $\varepsilon$, in the second equation while maintaining the overall effective viscosity.

The first equation of the standard model was modified to include a new constant $C_{k2}$. This constant reduces the (negative) source strength of dissipation in the turbulent kinetic energy equation:

$$\rho u\frac{\partial k}{\partial x}+\rho v\frac{\partial k}{\partial y}=\frac{\partial}{\partial x}\left[\left(\mu+\frac{\mu_t}{\sigma_k}\right)\frac{\partial k}{\partial x}\right]+\frac{\partial}{\partial y}\left[\left(\mu+\frac{\mu_t}{\sigma_k}\right)\frac{\partial k}{\partial y}\right]$$
$$+\mu_t\left[2\left(\frac{\partial u}{\partial x}\right)^2+2\left(\frac{\partial v}{\partial y}\right)^2+\left(\frac{\partial u}{\partial y}+\frac{\partial v}{\partial x}\right)^2\right]-C_{k2}\rho\varepsilon \quad (5)$$

The second equation was modified using the existing constant $\sigma_\varepsilon$. This constant was chosen for adjustment in an effort to reduce the dissipation of *dissipation*. By increasing $\sigma_\varepsilon$, the dissipation levels will increase to compensate for the reduction in $k$ caused by $C_{k2}$.

The adjustment process was monitored using the kinetic energy of turbulence of a node located at the center of the grid of the two-dimensional KEYO model. The kinetic energy of turbulence of this node was 0.001285 $m^2/s^2$ using the standard k-ε model without adjustments. In order to bring the velocity fluctuations $v'$ up to real levels, the turbulence must be increased by $(1/0.355)^2$ or about eight times. The center grid node should be 0.0102 $m^2/s^2$ after adjustment.

Figure 11 gives the range of adjustments to the constants $C_{k2}$ and $\sigma_\varepsilon$ that provided various levels of turbulent kinetic energy without drastically changing the velocity distribution.

As seen in Figure 11 the values of 0.77 for the new constant $C_{k2}$ and 1.67 for $\sigma_\varepsilon$ were the best for matching turbulent kinetic energy in the center of the model grid. The scattering of the fluctuating velocity $v'$ is plotted for all nodes in the simplified model using KEYO. The distribution in Figure 12 is much closer to that shown earlier in Figure 9.

The adjusted constants were applied over a Reynolds number range of half the cabin (Re/2) to twice the cabin (2 × Re) and found to be acceptable. A grid refinement of doubling the grid size resulted in about an 11% change in center node $k$, which is assumed to be sufficient.

Many CFD codes are not able to incorporate the new constant $C_{k2}$. For these codes, adjusting the turbulent kinetic energy in a post processing operation can make a good approximation for the constant $C_{k2}$. During the particulate phase of the solution, when all variables are held constant except for the particulate concentration, the turbulent kinetic energy can be multiplied uniformly by about eight times. This is probably the best approach until better models available or special user defined subroutines that can modify the turbulence are developed. Another possibility is to incorporate a very large molecular diffusion during the particulate modeling phase to compensate for the low predicted levels.

## CONCLUSIONS AND RECOMMENDATIONS

In this study, we have explored means to obtain the airflow characteristics using different CFD techniques. Due to the constraints of the available computing resources, simplified cabin models were built to capture the subtlety of the turbulence physics involved in aircraft cabins using LES. We

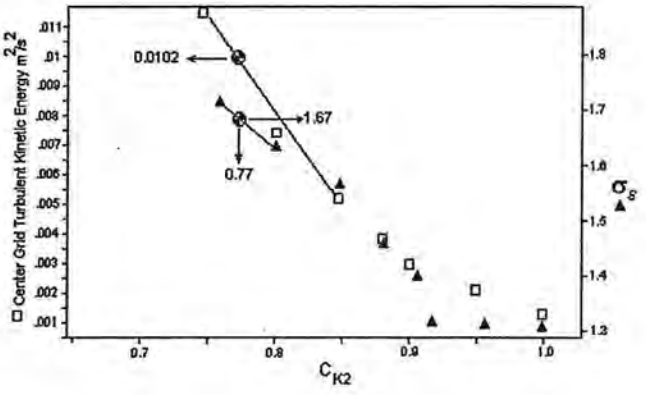


*Figure 11 Adjustments to turbulence model.*

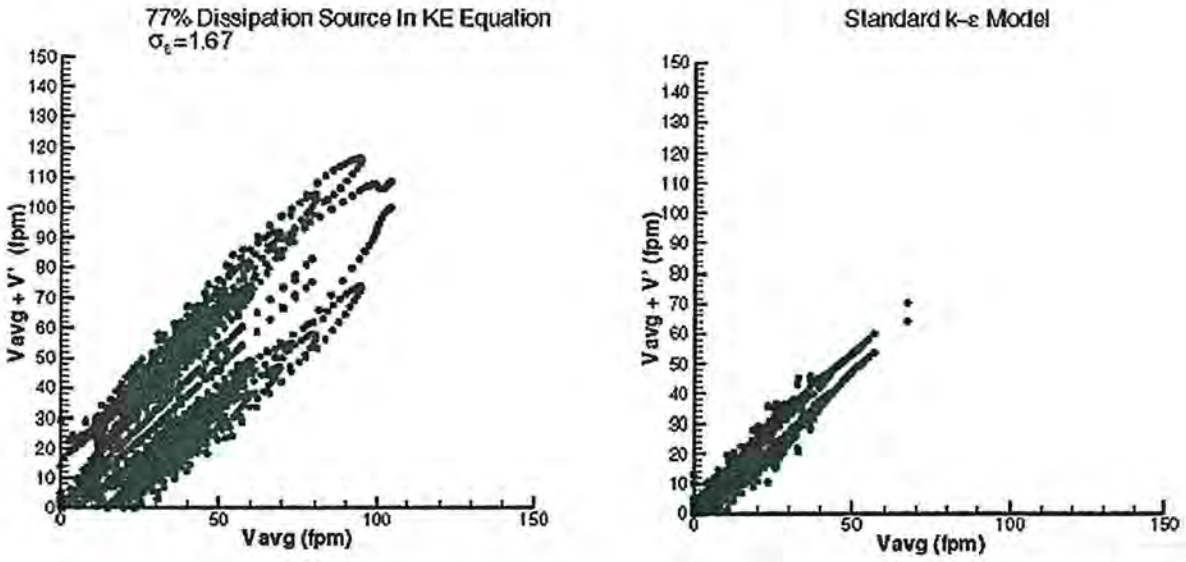


*Figure 12 A comparison of velocity after model adjustments.*

have confirmed the applicability of the LES results to the two-row section of a B767-300 cabin. The LES data obtained in this study also provide the essential airflow information to adjust our RANS simulations and the subsequent pathogen dispersion simulation for disease transmission (reported separately). We have demonstrated:

- The actual kinetic energy of turbulence as shown in LES and by measurement is approximately eight times larger than that predicted using the standard k-ε model. Since turbulent fluctuations are a prime factor in particle dispersion, standard k-ε models, such as RANS are unable to correctly predict disease dispersion.
- Simplified LES models with equivalent Reynolds numbers are accurate in predicting turbulence levels in dimensionally accurate aircraft cabin models.
- Large CFD models of aircraft cabins are only possible at this time using RANS techniques. The standard k-ε turbulence model can be adjusted in the diffusion phase to account for the underprediction of kinetic energy.
- Another constant is required for the k-ε model if accurate turbulence levels are to be predicted in the flow solution phase. A new constant $C_{k2}$ in the kinetic energy equation along with modified $\sigma_\varepsilon$ in the dissipation equation successfully predicted turbulence levels for a range of Reynolds numbers.
- A comparison can be made between turbulence models and LES by a scatter of $V_{ave}\pm v'$. Average velocity $V_{ave}$, is obtained from an identical grid solution for both cases. The scatter in instantaneous velocity is obtained by subtracting $v'$ and adding $v'$ to the mean velocity for the turbulence models. The scatter in instantaneous velocity is obtained from the spatial distribution of velocity at any time step after flow has been established for the LES. A time varying assessment of turbulence levels (numerical anemometer) for all nodes is virtually impossible at this time.

During the course of this study, several items worthy of further investigation have been identified:

- For the simplified cabin model, a test that produces high quality airflow data is needed to validate the CFD findings in this study. The experimental work is currently underway.
- The effect of aisle flow on the pathogen dispersion in aircraft cabins deserves further study.
- A study to simulate the dispersion of disease-laden aerosols in aircraft cabins using the multiphase approach is recommended to account for the multiphase effect of aerosols.
- Non-standard turbulence model adjustments should be benchmarked in full size laboratory tests.
- Direct coupling of network models to CFD models should be a future goal to allow for the real-time modification of the CFD boundary conditions to be evaluated.

## ACKNOWLEDGMENTS

The authors are sincerely grateful to Dr. Richard Griffith of Sandia National Laboratories in providing the computing resources for our three-dimensional LES work and Dr. M.H. Hosni of Kansas State University for his insights into this flow behavior. Within the Boeing Company, we would like to thank our colleague Dr. Ted Wu for verifying our LES results by performing a separate LES using the National Institute of Standards and Technology (NIST) developed fire dynamics

simulator (FDS). We are also indebted to Art Davenport and Jeanne Yu for their discussions and support of this work. Lee Briggs, Dean Rogers, and Jim Simek have encouraged and supported the publication of this work.

## NOMENCLATURE

AFT = aft of the cabin model
CFD = computational fluid dynamics
FDS = fire dynamics simulator
FWD = forward of the cabin model
$C_{\varepsilon 1}$ = constant = 1.45
$C_{\varepsilon 2}$ = constant = 1.92
$C_{\kappa 2}$ = constant = 1.0 for standard k-ε model and 1.67 for modified k-ε model
DNS = direct numerical simulation
$E_1$ = see definition in Equation 4
KEYO = a proprietary K-Epsilon stream function vorticity code
$k$ = turbulent kinetic energy
$l$ = turbulence length scale
LES = large eddy simulation
NIOSH = National Institute for Occupational Safety and Health
NIST = National Institute of Standards and Technology
RANS = Reynolds-averaged Navier-Stokes simulation
$P_{static}$ = static pressure
Re = Reynolds number
$Re_i$ = Reynolds number based on the characteristic length at inlet
RNG = renormalization group
SGS = sub-grid scale
$t$ = time
$T_{inlet}$ = supply air temperature at the air distribution nozzle
$u$ = fluid velocity in the x-direction
$V_{ave}$ = average velocity magnitude
$v$ = fluid velocity in the y-direction
$v'$ = fluctuating velocity
$|\bar{V}|$ = mean flow velocity magnitude
$|\vec{V}|$ = instantaneous flow velocity magnitude
$|v'|$ = flow fluctuation magnitude due to large eddy motion
$|v'|_{SGS}$ = the instantaneous velocity magnitude due to the sub-grid scale motion
$x$ = horizontal distance
$y$ = vertical distance

### Greek Symbols

$\Delta t$ = time step
ε = dissipation rate of turbulent kinetic energy
η = Kolmogorov length scale
ρ = density
$\sigma_\varepsilon$ = constant = 1.3
$\sigma_k$ = constant = 1.0
τ = Kolmogorov time scale
μ = dynamic viscosity
$\mu_t$ = eddy viscosity
ν = kinematic viscosity
$\nu_t$ = kinematic eddy viscosity

## REFERENCES

Aboosaidi, F., M.J. Warfield, and D. Choudhury. 1991. Numerical analysis of airflow in aircraft cabins, Technical Paper SAE 91-1441, SAE.

Baker, A.J., M.B. Taylor, N.S. Winowich, and M.R. Heller. 2000. Prediction of the distribution of indoor air quality and comfort in aircraft cabins using computational fluid dynamics. Air Quality and Comfort in Airliner Cabins, ASTM STP 1393, N. L. Nagda, Ed., ASTM.

Bjorn, E., and P.V. Nielson. 1998. CFD simulations of contaminant transport between two breathing persons, Vol. 2, pp.133-140, ROOMVENT '98, 6th International Conference on Air Distribution in Rooms, Stockholm, Sweden, June 14-17.

Chen, Q., A. Moser, and A. Huber. 1990. Prediction of buoyant, turbulent flow by a low reynolds-number k-ε Model. *ASHRAE Transactions* 96(1):564-573.

Chen, Q., and J. Srebric. 2001. How to verify, validate, and report indoor environment modeling CFD analyses, ASHRAE RP-1133, ASHRAE.

Emmerich, S.J., and K.B. McGrattan. 1998. Application of a large eddy simulation model to study room airflow. *ASHRAE Transactions* 104(1):1-9.

Fluent, Inc. 1998. *Fluent 5, User's Guide*.

Haghighat, F., J.C.Y. Wang, and Z. Jiang. 1989. Natural convection and airflow pattern in a partitioned room with turbulent flow *ASHRAE Transactions* 95(2):600-610.

Haghighat, F., J.C.Y. Wang, and Z. Jiang. 1990. Development of a three-dimensional numerical model to investigate the airflow and age distribution in a multizone enclosure. *Proceedings 5th International Conference on Indoor Air Quality and Climate: Indoor Air '90*, Vol. 4, pp.183-188, Ottawa, Ontario, Canada.

Haghighat, F., J.C.Y. Wang, Z. Jiang, and F. Allard. 1992. Air movement in buildings using computational fluid dynamics. *ASME Transactions, Journal of Solar Energy Engineering*, Vol. 114, pp.84-92.

Horstman, R.H. 1988. Predicting velocity and contaminant distribution in ventilated volumes using Navier-Stokes equations, ASHRAE Conference, IAQ 88, pp. 209-230.

Jin, G., and M. Braza. 1994. Two-equation turbulence model for unsteady separated flows around airfoils. *AIAA J.* 32(11):2316-2320.

Jones, B.W. 2000. The interaction of air motion and the human body in confined spaces, ASHRAE R-978, Kansas State University.

Lin, C.H., T. Han, and C.A. Koromilas. 1992. Effects of HVAC design parameters on passenger thermal comfort, *SAE Technical Paper* 920264, SAE.

Lin, C.H., et al. 2001. A numerical model for airborne disease transmission in a 767-300 passenger cabin, Final Report to the National Institute for Occupational Safety and Health. Contract #200-2000-08001. Boeing Commercial Airplanes Group.

Lo, L.-M. 1997. Numerical studies of airflow movement and contaminant transport in hospital operating rooms, M. Sc. Thesis, University of Minnesota.

Mathieu, J., and J. Scott. 2000. *An Introduction to Turbulent Flow*, pp.338-339, Cambridge University Press.

Mizuno, T., and M.J. Warfield. 1992. Development of three dimensional thermal airflow analysis computer program and verification test. *ASHRAE Transactions* 98(2):329-338.

Murakami, S., S. Kota, and Y. Suyama. 1988. Numerical and experimental study on turbulent diffusion fields in convection flow type clean rooms. *ASHRAE Transactions* 94(2):469-493.

Nielsen, P.V. 1974. Flow in air-conditioned rooms, Ph.D. thesis, Technical University of Denmark, Copenhagen.

Robinson, D.F., and H.A. Hassan. 1997. Modeling of separated turbulent flows, AIAA Paper 97-0207, 35th Aerospace Sciences Meeting & Exhibit, Reno, NV, January 6-10.

Zhang, W., and Q. Chen. 2000. Large eddy simulation of natural and mixed convection airflow indoors with two simple filtered dynamic subgrid scale models. *Numerical Heat Transfer* 37(A):447-463.

# OCLC FirstSearch: Display

Your requested information from your library BATTELLE MEM INST

Return

**PENDING - Lender**
**Record number: 3 Total records: 3**

*18783878*

## General Record Information

| | | | |
|---|---|---|---|
| **Request Identifier:** | **18783878** | **Status:** | PENDING 20060330 |
| **Request Date:** | 20060330 | **Source:** | FSILLSTF |
| **OCLC Number:** | 7182738 | | |
| **Borrower:** | **OSH** | **Need Before:** | 20060429 |
| **Receive Date:** | | **Renewal Request:** | |
| **Due Date:** | | **New Due Date:** | |
| **Lenders:** | *BKM, CWR, AKR, IRQ, KUK | | |

TH720 1. Am35t

## Bibliographic Information

Connect to the catalog at your library

| | |
|---|---|
| **Call Number:** | Lender's Holdings: 74-(1968-) |
| **Author:** | Lin, C et al. |
| **Title:** | ASHRAE transactions. |
| **ISSN:** | 0001-2505 |
| **Imprint:** | New York : American Society of Heating, Refrigerating and Air-Conditioning Engineers, 1968 9999 |
| **Article:** | Numerical simulation of airflow and airborne pathogen transport in aircraft cabins, Part 1: Numerical simulation of the flow field |
| **Volume:** | 111 |
| **Number:** | part 1 |
| **Date:** | 2005 |
| **Pages:** | 755-763 |
| **Verified:** | WorldCat CODEN: ASHTAG Desc: v. :Type: Serial |

## Borrowing Information

| | |
|---|---|
| **Patron:** | Bennett, Bill C-18 v |
| **Ship To:** | NIOSH Library/ILL Dept. C-21 Evelyn Palassis/4676 Columbia Pky/Cincinnati, OH 45226/(513) 533-8387 |
| **Bill To:** | same /PLEASE INCLUDE ILL # ON THE INVOICE |
| **Ship Via:** | Library Rate |
| **Maximum Cost:** | $35.00 |
| **Copyright Compliance:** | CCG |